Shahid Beheshti University

Sustainable Earth Trends

Journal homepage: http://sustainearth.sbu.ac.ir

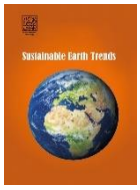

Evaluation of the efficiency of a multilayer photocatalyst in the removal of methylene blue

Asma JamiAlahmadi[a], Mahmood Hajiani[b*], Mohammad Hossein Sayadi[c]

[a] Department of Environmental Engineering, Faculty of Natural Resources and Environment, University of Birjand, Birjand, Iran
[b] Department of Civil Engineering, Faculty of Engineering, University of Birjand, Birjand, Iran
[c] Department of Environmental Science, Faculty of Natural Resources and Environment, Shahid Bahonar University of Kerman, Kerman, Iran

ABSTRACT

This study developed a two-layer structured photocatalyst, featuring a magnetic nickel core and a shell composed of a tin-based semiconductor and carbon nitride. The composite core was synthesized using a green approach, leveraging rosemary plant extract. A notable advantage of this photocatalyst is forming a floating layer through a gelation process, facilitated by freeze-drying, which creates internal pores. These pores not only enhanced the floatability of the structure but also improved light penetration into the nanoparticles, thereby increasing the photocatalytic efficiency of the synthesized composite. Structural characterization of the nanoparticles, including FESEM, XRD, EDX, and FTIR analyses, confirmed the successful synthesis of the proposed photocatalyst. FESEM analysis revealed that the average particle diameter was less than 1.5 micrometers. The photocatalyst's performance was assessed in a continuous reactor under UV irradiation for methylene blue degradation across varying conditions: pH levels (3, 5, 7, 9, and 11), catalyst dosages (0.2, 0.4, 0.6, 0.8, and 1 g/L), and initial dye concentrations (10, 20, 30, 40, and 50 mg/L). Optimization studies identified the optimal conditions for photocatalysis as a pH of 11, a photocatalyst dosage of 0.6 g/L, and an initial dye concentration of 50 mg/L. Under these conditions, the methylene blue removal efficiency reached 82%. Furthermore, reusability studies demonstrated that the core structure of the photocatalyst retained its essential properties and effectiveness in removing organic pollutants even after five reuse cycles.

ARTICLE INFO

Keywords:
Anionic dye
Core-shell structure
Natural polymer
Photocatalytic degradation

Article history:
Received: 01 Nov 2024
Accepted: 29 Nov 2024

*Corresponding author
E-mail address:
hajiani@birjand.ac.ir
(M. Hajiani)

Citation:
JamiAlahmadi, A. et al., (2025). Evaluation of the efficiency of a multilayer photocatalyst in the removal of methylene blue, *Sustainable Earth Trends:* 5(4), (1-10).

DOI: 10.48308/set.2024.237678.1088

1. Introduction

Environmental pollution is one of the most pressing challenges confronting modern society. It encompasses a wide range of pollutants, including chemicals, waste materials, light, heat, sound, and other harmful factors (Sadia et al., 2023). Both natural and synthetic dyes are chemical substances widely used across various industries. While dyes hold significant commercial value, their excessive discharge into aquatic ecosystems can result in severe environmental and health issues (Lee and Kwon, 2023). Numerous industries, such as textiles, cosmetics, paper, tanning, leather, and plastics, release substantial amounts of dyes into the environment, contributing to pollution and ecological imbalance (Ullah Khan et al., 2023), leading to pollution, particularly in water sources. Dyes are among the most hazardous groups of chemical compounds present in industrial wastewater. Their significance lies in their ability to obstruct light penetration, thereby disrupting photosynthesis in aquatic ecosystems (Lima et al., 2008; Royer et al., 2009). Industrial wastewater often contains a mix of chemicals, suspended solids, toxic substances, and dyes, which are the most immediately visible pollutants to the human eye. Organic dyes, owing to the presence of aromatic compounds, salts, and chlorides, are particularly toxic to aquatic life, leading to their

mortality (Khosravi Mohammad Soltan et al., 2021; Koyuncu, 2002). Therefore, to safeguard human health and protect the environment, it is crucial to implement effective methods for removing dyes from wastewater.

Advanced Oxidation Processes (AOPs), including photocatalysis, are recognized as effective technologies capable of converting pollutant molecules into mineral substances under light exposure (Ji et al., 2020; Daliri et al., 2024). Photocatalytic materials are created by transforming metal and non-metal semiconductors into colloidal materials (ranging from 10 to 100 nanometers) and nanoscale nanoclusters (less than 10 nanometers) (Mohamed et al., 2012). When a photon with energy equal to or greater than the bandgap of the light-absorbing semiconductor photocatalyst is absorbed, it triggers the initiation of a photocatalytic reaction (Van Gerven et al., 2007; Hajiani et al., 2022b). This reaction causes an electron to be excited from the valence band to the conduction band, generating an excited electron in the conduction band and a positive hole in the valence band (Chong et al., 2010). Due to its advantages over traditional methods—such as rapid oxidation, the absence of polycyclic product formation, the ability to oxidize pollutants at low concentrations, and the production of harmless byproducts—this process has become one of the most promising methods for wastewater treatment (Pouretedal et al., 2009; Hajiani et al., 2022a).

Despite the advantages of photocatalytic degradation processes, several challenges and limitations exist in their application. Small photocatalytic nanoparticles are susceptible to aggregation, which diminishes the surface area available for light exposure (Shan et al., 2010), This aggregation reduces photocatalytic efficiency. Additionally, the deposition of powdered photocatalysts in polluted solutions significantly diminishes the number of photons available to the catalysts. Although phase separation technology is commonly employed to recover powdered photocatalysts after use, it is time-consuming and inefficient. Inadequate separation and recycling of photocatalysts can also result in secondary pollution (Jbeli et al., 2018; Mallakpour et al., 2019).

To overcome the challenges associated with powdered photocatalysts, the development of floating photocatalysts provides a promising solution. These materials offer several advantages, such as enhanced photocatalytic oxygenation at the air/water interface, high light quantum efficiency, superior dispersion, and ease of recycling (Xue et al., 2016; Dalponte et al., 2019). Photocatalysts made from various materials, including synthetic polymers, have been employed to impart floating properties (Huang et al., 2021), However, the slow degradation of synthetic polymers may present environmental challenges.

In this study, a two-layer core-shell structured heterogeneous photocatalyst system was developed and synthesized. The system features floating alginate/Nickel Ferrite spheres as the core photocatalyst carrier, with tin dioxide and graphitic carbon nitride as the shell materials. The photocatalytic performance of the synthesized photocatalysts was assessed using methylene blue (MB) as a model pollutant under UV irradiation. Key parameters, including pH, dye concentration, and photocatalyst dosage, were investigated and optimized. Furthermore, the stability of the photocatalytic efficiency was evaluated over five reuse cycles under the optimized conditions.

2. Material and methods

2.1. Chemicals

Melamine ($C_3H_6N_6$) (98%), tin(II) chloride dihydrate ($SnCl_2{\cdot}2H_2O$, MW = 225.63 g/mol), calcium chloride dihydrate ($CaCl_2{\cdot}2H_2O$, MW = 147.02 g/mol), polyvinylpyrrolidone (PVP, C_6H_9NO), ferric chloride hexahydrate ($FeCl_3{\cdot}6H_2O$, MW = 270.33 g/mol), and nickel(II) chloride hexahydrate ($NiCl_2{\cdot}6H_2O$, MW = 237.69 g/mol) were obtained from Merck, Germany. The biopolymer sodium alginate (CAS 9005-38-3) with viscosity < 2000 was sourced from Sigma-Aldrich, Germany. Methylene blue dye (molecular weight 319.85 g/mol, chemical formula $C_{16}H_{18}N_3SCl$) was purchased from Alvan Sabet Co., Qazvin. Sodium hydroxide, hydrochloric acid, sodium chloride (NaCl), and deionized water (DI) were used in the experiments. Rosemary leaves were collected from the green spaces of Birjand University.

2.2. Instruments

X-ray diffraction (XRD) analysis was performed using a device manufactured in the Netherlands (XRD Philips PW1730). For FTIR

spectroscopy, a JASCO spectrometer from Japan was used. For structural analysis, a TESCAN MIRA3 scanning electron microscope (SEM) from the Czech Republic was used. X-ray photoelectron spectroscopy (XPS) analysis was performed using an instrument from SPECS (Berlin, Germany) for further structural studies of the nanoparticles. For measuring the concentration of the pollutant, a UV-Vis spectrophotometer (Shimadzu Biospec 1601, Japan) was used.

2.3 Synthesis of heterostructured graphitic carbon nitride nanosheets and tin oxide

Graphitic carbon nitride nanosheets synthesized by (Yang et al., 2013) were used for the fabrication of tin oxide shells. Initially, a specific amount of graphitic carbon nitride nanosheets was thoroughly mixed with distilled water using ultrasonication. Subsequently, $SnCl_2 \cdot 2H_2O$ and PVP were added to the mixture. The resulting suspension was rapidly stirred and then transferred into a Teflon-lined autoclave to undergo a hydrothermal reaction. The resulting material was cooled to room temperature, washed with deionized water, centrifuged, and finally dried (Huang et al., 2015).

Rosemary plant extract was used to synthesize the proposed nanoparticles for the composite core. Specific amounts of $FeCl_3 \cdot 6H_2O$ and $NiCl_2 \cdot 6H_2O$ were added to the prepared extract and stirred thoroughly. The pH of the mixture was adjusted using NaOH. Finally, the resulting nanoparticles were washed with deionized water and alcohol and then placed in an oven for drying (Alijani et al., 2020). To fabricate the proposed core-shell floating structure, the core nanoparticles were first dissolved in deionized water, followed by the addition of sodium alginate to the solution. The mixture was stirred and then added dropwise to a $CaCl_2$ solution. The resulting spheres were washed with deionized water. Subsequently, the synthesized shell was mixed with sodium alginate in deionized water and stirred thoroughly. The resulting alginate mixture, along with the alginate-containing core from the previous step, was passed through a perforated plastic mold into a $CaCl_2$ solution. The resulting spheres, after being washed with deionized water, were placed in a freeze-dryer.

2.4. Photocatalytic experiments

To evaluate the photocatalytic activity of the synthesized catalyst, a batch reactor equipped with a UV lamp was used. In this reactor, a specified amount of a methylene blue solution with a known concentration and a fixed amount of photocatalyst were irradiated. Then, at regular time intervals, a sample of the solution was taken from the reactor, and the remaining pollutant concentration was measured using a spectrophotometer. The adsorption capacity under dark conditions and the amount of photolysis were also determined. The removal efficiency of the pollutant was calculated using the following Eq. 1:

$$\text{Removal Efficiency } (\%) = \frac{C_0 - C_t}{C_0} \qquad (1)$$

Where:

C_0 is the initial concentration of the pollutant (before irradiation).

C_t is the concentration of the pollutant at time t (after irradiation).

Additionally, the experiments were conducted as a time-dependent factor. First, the optimal pH value was determined. Then, using this optimal pH, the optimal photocatalyst dosage was identified. After that, based on the previously determined optimal values, the optimal concentration of the pollutant was established.

2.5. Optimization of factors affecting the photocatalytic process

In this study, the factors influencing the photocatalytic process were optimized. First, the optimal pH was determined from values of 3, 5, 7, 9, and 11. To adjust the pH of the solutions, 0.1 M HCl and NaOH were used. Subsequently, the optimal photocatalyst dosage was identified from 0.2, 0.4, 0.6, 0.8, and 1 g/L. Finally, with the process adjusted to the optimal pH and catalyst dosage, the optimal pollutant concentration was selected from 10, 20, 30, 40, and 50 mg/L. Sampling was performed at 60, 90, and 120 minutes after the initiation of the photocatalytic process and the activation of the UV lamp. It is worth mentioning that the reactor was completely covered with aluminum foil to prevent light from entering.

3. Results and discussion

3.1. FESEM

The morphology and microstructure of the final product were examined using Field Emission Scanning Electron Microscopy (FE-SEM). The presence of cavities resulting from the photocatalyst drying process using a freeze-dryer is clearly visible in the images. One of the advantages of these cavities is the enhanced photocatalytic activity of the synthesized composite due to the penetration of light into the cavities and the increased excitation of electrons in the valence band. Due to this structure, the possibility of generating electron-hole pairs is greater compared to other photocatalysts. The average particle diameter was less than 1.5 micrometers (Fig.1).

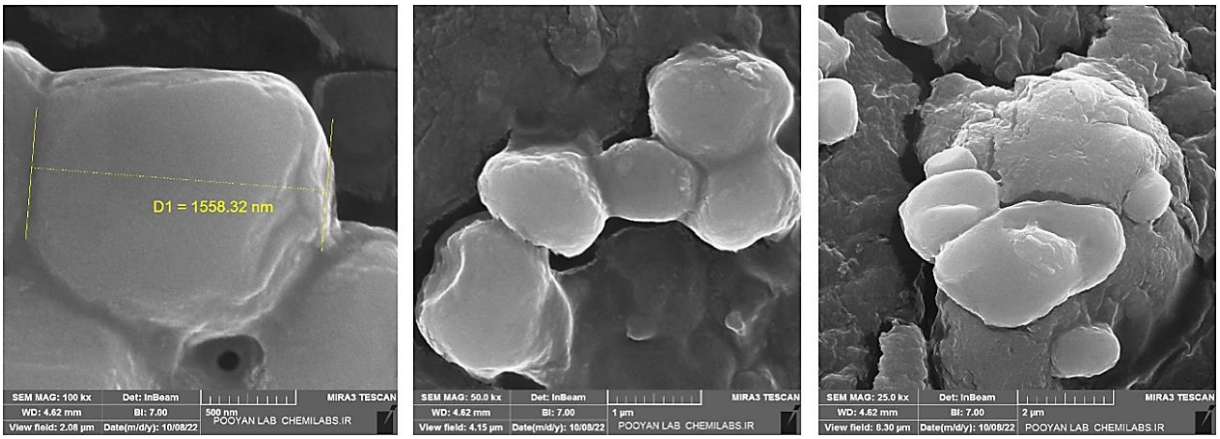

Fig.1. FESEM images of photocatalyst.

3.2. X-ray diffraction (XRD)

The phase and crystal structure of the final molecule were determined through XRD analysis. The XRD pattern is presented in Fig. 2. Two peaks in the XRD spectrum of Sn-CN@NFO-SA were observed at 2θ diffraction angles of 13° and 22°, which have previously been attributed to the amorphous nature of calcium alginate (Larosa et al., 2018). A strong peak observed at 29.95° corresponds to the graphite planes of carbon nitride, reflecting the aromatic system of these planes (Mamba and Mishra; 2016, Wang et al., 2018). Additionally, the planes corresponding to tin oxide are observable at peaks of 33.3° and 57.5°, which are slightly shifted in the final nanocomposite structure(Kumar et al., 2022, Zeng et al., 2019). Reflections corresponding to $NiFe_2O_4$ are observed at angles of 35.55°, 45.45°, and 58.8° (Bameri et al., 2022).

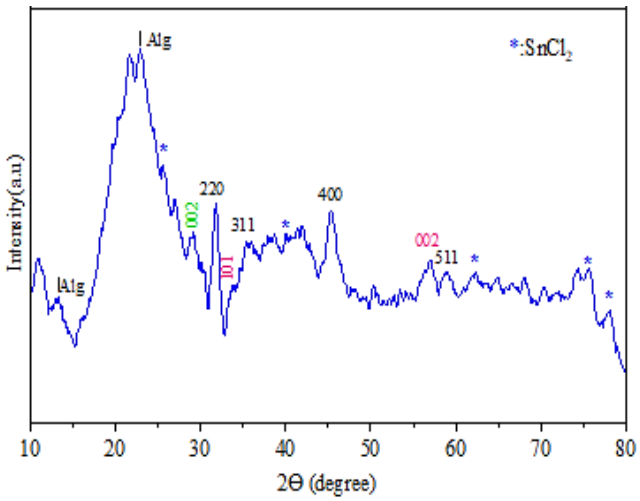

Fig. 2. The X-ray diffraction spectrum of the synthesized photocatalyst.

3.3. Fourier Transform Infrared (FTIR) spectrum

The Fourier Transform Infrared (FTIR) spectrum of the final molecule sample is presented in Fig. 3. The weak peak in the range of 1300–1700 cm^{-1} is primarily attributed to the stretching bonds of C–N and C=N (43). Additionally, two characteristic bands located in the range of 1000–1200 cm^{-1} were identified as the stretching vibrations of C–O–C and C–C bonds (Fila et al., 2022). This peak indicates the presence of amine groups originating from g-C_3N_4 within the molecular framework of the composite. In the range of 500–600 cm^{-1}, stretching bonds of C–Cl are observed. In the range of 1500–1750 cm^{-1}, a peak corresponding to the asymmetric stretching vibrations of COO groups is observed, indicating the presence of carboxylate functional groups.

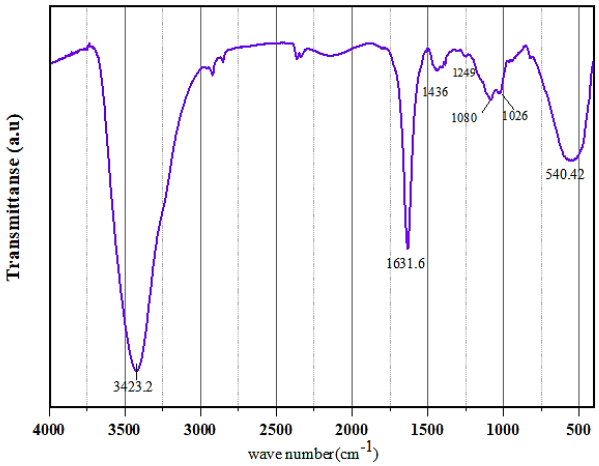

Fig. 3. FTIR spectrum of a catalyst.

3.4. Energy Dispersive X-ray Spectroscopy (EDX) analysis

Energy Dispersive X-ray Spectroscopy (EDX) analysis of the final product was performed to evaluate its elemental composition, and the results are shown in Fig. 4. As seen in the image, the presence of tin, nickel, and iron elements indicates the successful synthesis of the desired catalyst. Additionally, the presence of elements such as C, O, N, and Cl provides strong evidence of the successful completion of the synthesis steps. The presence of calcium and sodium further confirms the gel formation process, which is facilitated by sodium alginate salts and $CaCl_2$, thereby supporting the structural features of the product.

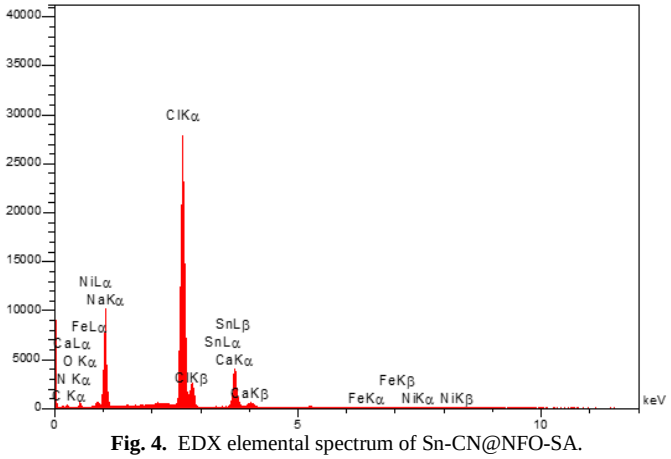

Fig. 4. EDX elemental spectrum of Sn-CN@NFO-SA.

3.5. Photocatalytic activity

3.5.1. Optimization of pH

One of the most important factors in chemical reactions is the pH of the environment. The primary effect of this parameter is on the surface charges generated, such that numerous studies have shown that changes in pH significantly influence the efficiency of pollutant removal (Rajabi et al., 2016). This parameter is also crucial in the photocatalytic process, as the adsorption of pollutants on the

catalyst surface and the continuation of the process are highly dependent on pH. After adjusting the selected pH levels (3, 5, 7, 9, and 11), the photocatalyst was added to the solution. The photocatalytic activity was measured using the described method. As shown in Fig. 5, the optimal degradation efficiency of MB occurred at pH 11. As seen in the figure, the pollutant removal is higher at basic pH values than at acidic ones. Since MB is a cationic dye, at low pH, the competition between the positive charge in the solution and the MB dye can hinder sufficient contact between MB and the photocatalyst. In general, at higher pH, the surface charge of the photocatalyst becomes less positive. As a result, MB can be adsorbed onto the photocatalyst surface, allowing a greater extent of degradation to occur (Faraji et al., 2021).

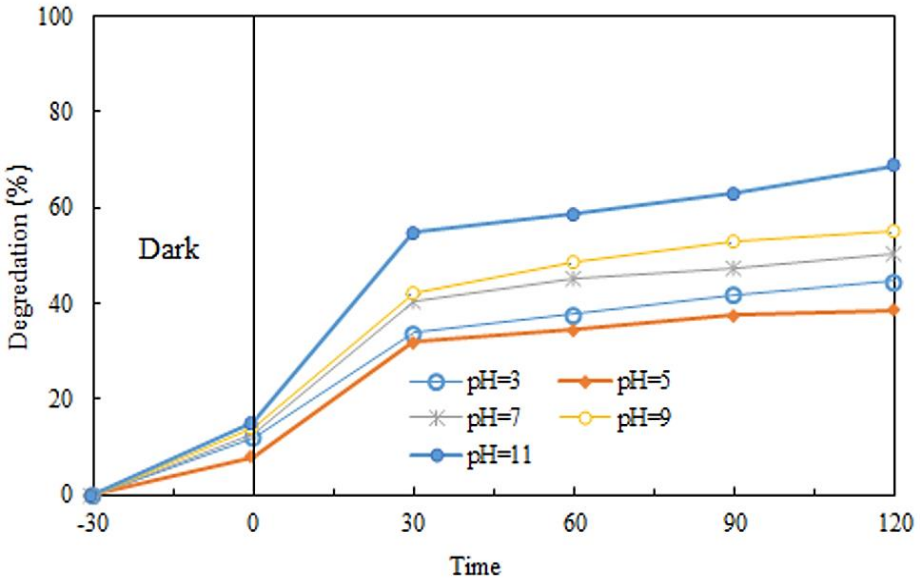

Fig. 5. Effect of pH on photocatalytic degradation of methylene blue dye.

3.5.2. Optimization of photocatalyst dosage

The next step was to determine the optimal dosage of the photocatalyst. Since the available sites for the photocatalytic process depend on the catalyst dosage, changing the amount of catalyst affects the efficiency of the process (Juang et al., 2010). In this stage, the pH was set to 11, and the proposed catalyst dosages were added to the reactor in separate experiments to determine the optimal photocatalyst dosage. Based on the results obtained and as shown in Fig. 6, the optimal photocatalyst amount was found to be 0.6 g/L, meaning that the optimal photocatalytic degradation rate of MB occurred at an intermediate concentration of the photocatalyst. As the concentration of the photocatalyst increases, more surface sites become available for the degradation reaction, leading to more collisions between the pollutant and the catalyst. However, at very high concentrations, due to the high aggregation of molecules, light penetration is reduced, and as a result, the photocatalytic degradation efficiency also decreases. On the other hand, at low photocatalyst concentrations, fewer active sites are available for the pollutants, which in turn reduces the degradation efficiency. Therefore, the best photocatalytic degradation occurs at an intermediate photocatalyst concentration. In a study by Saho and Gupta on the removal of methylene blue (MB) using silver-ion-doped titanium dioxide, it was found that the optimal photocatalyst dosage for effective removal lies within the intermediate range (Sahoo and Gupta, 2012).

3.5.3. Optimization of initial pollutant concentration

The initial concentration of the dye significantly influences the efficiency of the photocatalyst. The effect of MB concentration on degradation performance is illustrated in Fig. 7. As observed in Fig. 7, the degradation efficiency of MB improves over time for most

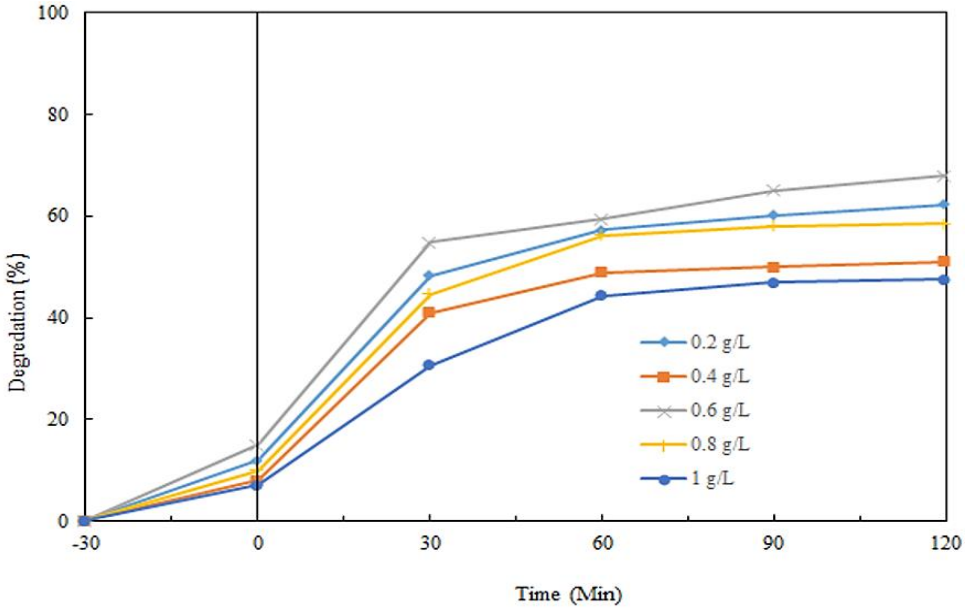

Fig. 6. Effect of photocatalyst concentration on MB degradation.

dye concentrations. Specifically, at a concentration of 10 mg/L, the degradation rate of MB increases markedly during the initial reaction period up to 60 minutes. However, between 60 and 90 minutes, the degradation rate slows, and between 90 and 120 minutes, it exhibits minimal further improvement, ultimately reaching approximately 58%. At MB concentrations of 30 and 40 mg/L, the degradation rate initially increases noticeably, but after 30 minutes, the degradation process stabilizes, and no significant further decomposition occurs. Similarly, at an MB concentration of 50 mg/L, the degradation rate intensifies sharply within the first 30 minutes, after which the degradation progresses at a slower pace, reaching approximately 82% after 120 minutes. Therefore, as demonstrated in Fig. 8, the best photocatalytic performance is observed at an MB concentration of 50 mg/L, the highest among the tested concentrations. Sahoo and Gupta identified an initial methylene blue dye concentration of 50 mg/L as the optimal value for photodegradation using a composite photocatalyst (Sahoo and Gupta, 2012). This result is advantageous for water consumption during MB removal using the synthesized photocatalyst, as achieving such a dye concentration in wastewater is sufficient to ensure high removal efficiency.

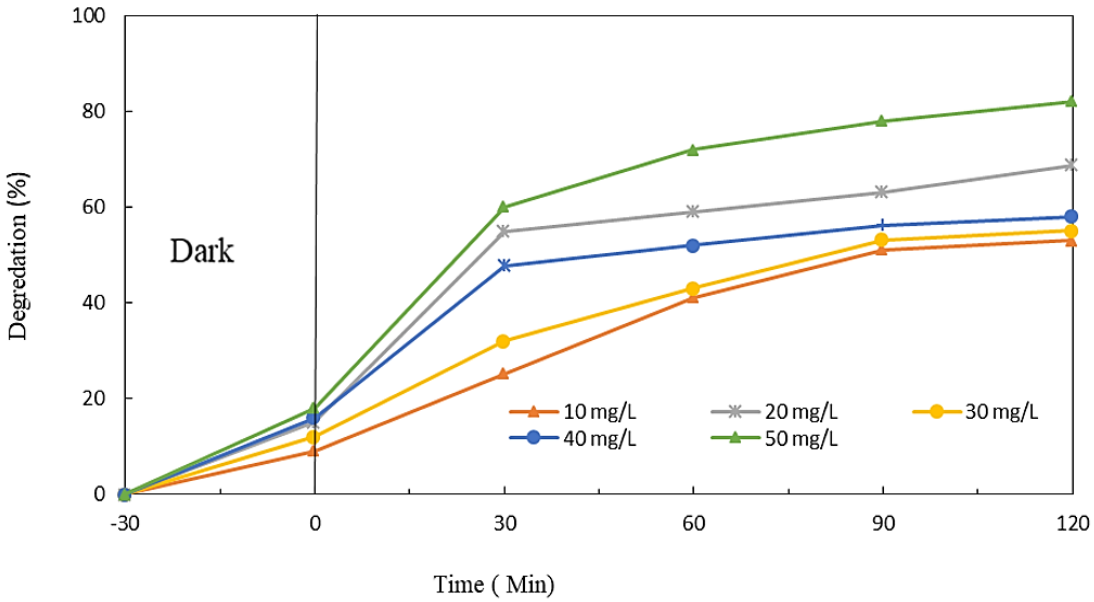

Fig. 7. Effect of initial MB concentration on removal efficiency.

3.6. Recyclability and reusability of the photocatalyst

To evaluate the stability and recyclability of the photocatalyst, recycling experiments were conducted over five cycles. After each cycle, the photocatalyst samples were recovered, thoroughly washed multiple times with deionized water to remove residual dye solution from the surface, and dried at room temperature for use in the subsequent experimental cycle. The results of the reuse experiments for MB degradation are presented in Fig. 8. As shown in the figure, the photocatalyst's degradation efficiency for MB removal decreases after five cycles, reaching approximately 60%. This reduction can likely be attributed to the degradation or weakening of some functional groups within the structure of the synthesized photocatalyst. Nevertheless, the results confirm that the main structure of the catalyst remains unchanged (Hajiani et al., 2023).

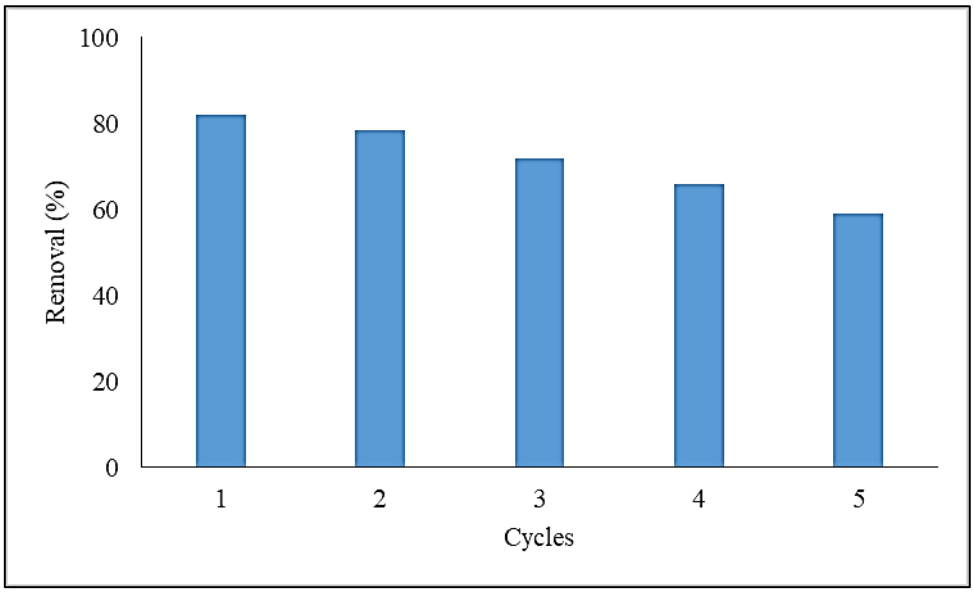

Fig. 8. Removal after 5 recycling.

4. Conclusion

In this study, a core-shell composite nanoparticle was synthesized for the photodegradation of methylene blue. To enable easy recovery from the reaction medium, a magnetic core was incorporated into the nanocomposite. A key advantage of this photocatalyst is its ability to float on the surface, which is facilitated by pores formed during freeze-drying. These pores enhance the buoyancy of the core-shell structure, improving oxygen access and photon utilization efficiency—both critical factors in accelerating pollutant degradation. The incorporation of the biopolymer alginate as a photocatalyst carrier not only strengthens the core-shell structure but also enhances the composite's environmental compatibility, addressing concerns related to disposal. Structural analyses, including FESEM, XRD, FTIR, and EDX, confirmed the successful synthesis of the photocatalyst. Following synthesis, the catalyst's ability to remove organic pollutants was evaluated in a batch reactor. Optimization experiments identified the ideal conditions for photocatalysis. Under these optimal conditions—pH 11, a nanoparticle dosage of 0.6 g/L, and an initial pollutant concentration of 50 mg/L—the photocatalyst achieved an 82% removal efficiency for methylene blue. Furthermore, its performance remained satisfactory after five consecutive reuse cycles. In conclusion, the use of the natural polymer alginate, with its biodegradability and environmental safety, demonstrates significant potential as a carrier material for various photocatalysts, offering both sustainability and enhanced performance.

Acknowledgements

The paper is from a PhD thesis in the Department of Environmental Engineering, Faculty of Natural Resources and Environment, University of Birjand. The authors feel it necessary to express their gratitude to the University of Birjand for its financial and moral support throughout all stages of this research, particularly to Engineer Shekari, and for providing access to the Central Environmental Laboratory of the Faculty of Natural Resources and Environment.

References

Alijani, H.Q., Pourseyedi, S., Torkzadeh-Mahani, M., Seifalian, A. & Khatami, M., 2020. Bimetallic nickel-ferrite nanorod particles: greener synthesis using rosemary and its biomedical efficiency. *Artificial Cells, Nanomedicine, and Biotechnology*, 48**,** 242-251.

Bameri, I., Saffari, J., Baniyaghoob, S. & Ekrami-Kakhki, M.-S., 2022. Synthesis of magnetic nano-NiFe2O4 with the assistance of ultrasound and its application for photocatalytic degradation of Titan Yellow: Kinetic and isotherm studies. *Colloid and Interface Science Communications*, 48**,** 100610.

Chong, M.N., Jin, B., Chow, C.W. & Saint, C., 2010. Recent developments in photocatalytic water treatment technology: a review. *Water Research*, 44**,** 2997-3027.

Daliri, M., Sayadi, M.H. & Hajiani, M., 2024. Developing the glycerol carbonylation process using photocatalysis and 2-cyanopyridine as a water-reducing agent. Sustainable Earth Trends, 4(4), 73-82.

Dalponte, I., De Sousa, B.C., Mathias, A.L. & Jorge, R.M.M., 2019. Formulation and optimization of a novel TiO2/calcium alginate floating photocatalyst. *International Journal of Biological Macromolecules*, 137, 992-1001.

Faraji, A., Mehrdadi, N., Mahmoodi, N.M., Baghdadi, M. & Pardakhti, A., 2021. Enhanced photocatalytic activity by synergic action of ZIF-8 and NiFe2O4 under visible light irradiation. *Journal of Molecular Structure*, 1223, 129028.

Fila, D., Hubicki, Z. & Kołodynska, D., 2022. Applicability of new sustainable and efficient alginate-based composites for critical raw materials recovery: General composites fabrication optimization and adsorption performance evaluation. *Chemical Engineering Journal*, 446, 137245.

Hajiani, M., Ezami, E. & Rezaei, M.R., 2022a. Photodegradation of Human Serum Albumin by Fe3O4/ZnO/Ag Nanocomposite. *Journal of Water and Environmental Nanotechnology*, 7(2), 132-142.

Hajiani, M., Gholami, A. & Sayadi, M.H., 2022b. Removal of pharmaceutical pollutants from aquatic environments using heterogeneous photocatalysis. *Advances in Environmental Technology*, 8(4), 271-278.

Hajiani, M., Sayadi, M.H., Mozafarjalali, M. & Ahmadpour, N., 2023. Green synthesis of recyclable, cost-effective, chemically stable, and environmentally friendly CuS@ Fe3O4 nanoparticles for the photocatalytic degradation of dye. *Journal of Cluster Science*, 34(4), 1939-1951.

Huang, S., Xu, Y., Xie, M., Xu, H., He, M., Xia, J., ... & Li, H., 2015. Synthesis of magnetic CoFe2O4/g-C3N4 composite and its enhancement of photocatalytic ability under visible-light. *Colloids and Surfaces A: Physicochemical and Engineering Aspects*, 478**,** 71-80.

Huang, X. H., Hu, T., Bu, H., Li, W. X., Li, Z. L., Hu, H. J., ... & Jiang, G.B., 2021.Transparent floatable magnetic alginate sphere used as photocatalysts carrier for improving photocatalytic efficiency and recycling convenience. *Carbohydrate polymers*, 254**,** 117281.

Jbeli, A., Hamden, Z., Bouattour, S., Ferraria, A.M., Conceicao, D.S., Ferreira, L.V., ... & Boufi, S., 2018. Chitosan-Ag-TiO2 films: an effective photocatalyst under visible light. *Carbohydrate polymers*, 199**,** 31-40.

Ji, M., Di, J., Liu, Y., Chen, R., Li, K., Chen, Z., ... & Li, H., 2020. Confined active species and effective charge separation in Bi4O5I2 ultrathin hollow nanotube with increased photocatalytic activity. *Applied Catalysis B: Environmental*, 268**,** 118403.

Juang, R.-S., Lin, S.-H. & Hsueh, P.-Y. 2010. Removal of binary azo dyes from water by UV-irradiated degradation in TiO2 suspensions. *Journal of Hazardous Materials*, 182**,** 820-826.

Khosravi Mohammad Soltan, F., Hajiani, M., & Haji, A., 2021. Nylon-6/poly (propylene imine) dendrimer hybrid nanofibers: An effective adsorbent for the removal of anionic dyes. *The Journal of The Textile Institute*, 112**,** 444-454.

Koyuncu, I. 2002. Reactive dye removal in dye/salt mixtures by nanofiltration membranes containing vinylsulphone dyes: effects of feed concentration and cross flow velocity. *Desalination*, 143**,** 243-253.

Kumar, J.V., Ajarem, J.S., Allam, A.A., Manikandan, V., Arulmozhi, R., & Abirami, N., 2022. Construction of SnO2/g-C3N4 an effective nanocomposite for photocatalytic degradation of amoxicillin and pharmaceutical effluent. *Environmental Research*, 209**,** 112809.

Larosa, C., Salerno, M., de Lima, J.S., Meri, R.M., da Silva, M.F., de Carvalho, L.B. & Converti, A., 2018. Characterisation of bare and tannase-loaded calcium alginate beads by microscopic, thermogravimetric, FTIR and XRD analyses. *International journal of biological macromolecules*, 115**,** 900-906.

Lee, J. & Kwon, K.H. 2023. Considering the risk of a coloring shampoo with the function of gray hair cover cosmetology and skin barrier: A systematic review. *Health Science Reports*, 6**,** e1271.

Lima, E.C., Royer, B., Vaghetti, J.C., Simon, N.M., da Cunha, B.M., Pavan, F.A., ... & Airoldi, C., 2008. Application of Brazilian pine-fruit shell

as a biosorbent to removal of reactive red 194 textile dye from aqueous solution: kinetics and equilibrium study. *Journal of Hazardous Materials*, 155(3), 536-550.

Mallakpour, S., Behranvand, V. & Mallakpour, F., 2019. Synthesis of alginate/carbon nanotube/carbon dot/fluoroapatite/TiO2 beads for dye photocatalytic degradation under ultraviolet light. *Carbohydrate polymers*, 224**,** 115138.

Mamba, G. & Mishra, A., 2016. Graphitic carbon nitride (g-C3N4) nanocomposites: a new and exciting generation of visible light driven photocatalysts for environmental pollution remediation. *Applied Catalysis B: Environmental*, 198**,** 347-377.

Mohamed, R., Mckinney, D. & Sigmund, W., 2012. Enhanced nanocatalysts. *Materials Science and Engineering: R: Reports*, 73**,** 1-13.

Pouretedal, H.R., Eskandari, H., Keshavarz, M.H., & Semnani, A., 2009. Photodegradation of Organic Dyes using Nanoparticles of Cadmium Sulfide Doped with Manganese, Nickel and Copper as Nanophotocatalyst. *Acta Chimica Slovenica*, 56.

Rajabi, H.R., Shahrezaei, F. & Farsi, M., 2016. Zinc sulfide quantum dots as powerful and efficient nanophotocatalysts for the removal of industrial pollutant. *Journal of Materials Science: Materials in Electronics*, 27**,** 9297-9305.

Royer, B., Cardoso, N.F., Lima, E.C., Vaghetti, J.C., Simon, N.M., Calvete, T. & Veses, R.C., 2009. Applications of Brazilian pine-fruit shell in natural and carbonized forms as adsorbents to removal of methylene blue from aqueous solutions—Kinetic and equilibrium study. *Journal of Hazardous Materials*, 164, 1213-1222.

Sadia, M., Ahmad, I., Ul-Saleheen, Z., Zubair, M., Zahoor, M., Ullah, R., ... & Zekker, I., 2023. Synthesis and characterization of MIPs for selective removal of textile dye acid black-234 from wastewater sample. *Molecules*, 28**,** 1555.

Sahoo, C. & Gupta, A., 2012. Optimization of photocatalytic degradation of methyl blue using silver ion doped titanium dioxide by combination of experimental design and response surface approach. *Journal of Hazardous Materials*, 215**,** 302-310.

Shan, A.Y., Ghazi, T.I.M. & Rashid, S.A., 2010. Immobilisation of titanium dioxide onto supporting materials in heterogeneous photocatalysis: A review. *Applied Catalysis A: General*, 389**,** 1-8.

Ullah Khan, A., Zahoor, M., Ur Rehman, M., Ikram, M., Zhu, D., Naveed Umar, M., ... & Ali, E.A., 2023. Bioremediation of azo dye Brown 703 by Pseudomonas aeruginosa: an effective treatment technique for dye-polluted wastewater. *Microbiology Research*, 14**,** 1049-1066.

Van Gerven, T., Mul, G., Moulijn, J. & Stankiewicz, A., 2007. A review of intensification of photocatalytic processes. *Chemical Engineering and Processing: Process Intensification*, 46(9), 781-789.

Wang, Q., Wang, W., Zhong, L., Liu, D., Cao, X., & Cui, F., 2018. Oxygen vacancy-rich 2D/2D BiOCl-g-C3N4 ultrathin heterostructure nanosheets for enhanced visible-light-driven photocatalytic activity in environmental remediation. *Applied Catalysis B: Environmental*, 220**,** 290-302.

Xue, H., Jiang, Y., Yuan, K., Yang, T., Hou, J., Cao, C., ... & Wang, X., 2016. Floating photocatalyst of B–N–TiO2/expanded perlite: a sol–gel synthesis with optimized mesoporous and high photocatalytic activity. *Scientific Reports*, 6(1), 29902.

Yang, S., Gong, Y., Zhang, J., Zhan, L., Ma, L., Fang, Z., ... & Ajayan, P.M., 2013. Exfoliated graphitic carbon nitride nanosheets as efficient catalysts for hydrogen evolution under visible light. *Advanced Materials*, 25(17), 2452-2456.

Zeng, J., Peng, C., Wang, R., Liu, Y., Wang, X. & Liu, J., 2019. Large-scale synthesis of hierarchical SnO spheres assisted with poly (N-isopropylacrylamide) for high lithium storage capacity. *Ceramics International*, 45(1), 1246-1250.